Discovery of Conical Intersection Mediated Photochemistry with Growing String Methods

Journal:	*Physical Chemistry Chemical Physics*
Manuscript ID	CP-ART-07-2018-004703.R1
Article Type:	Paper
Date Submitted by the Author:	04-Oct-2018

Complete List of Authors:	Aldaz, Cody; University of Michigan, Department of Chemistry Kammeraad, Joshua; University of Michigan, Department of Chemistry Zimmerman, Paul; University of Michigan, Chemistry

Discovery of Conical Intersection Mediated Photochemistry with Growing String Methods

Cody Aldaz, Josh Kammeraad, and Paul M. Zimmerman*
Department of Chemistry, University of Michigan, Ann Arbor, MI 48109
* Correspondence to *paulzim@umich.edu*

Abstract:

Conical intersections (CIs) are important features of photochemistry that determine yields and selectivity. Traditional CI optimizers require significant human effort and chemical intuition, which typically restricts searching to only a small region of the CI space. Herein, a systematic approach utilizing the growing string method is introduced to locate multiple CIs. Unintuitive MECI are found using driving coordinates that can be generated using a combinatorial search, and subsequent optimization allows reaction pathways, transition states, products, and seam-space pathways to be located. These capabilities are demonstrated by application to two prototypical photoisomerization reactions and the dimerization of butadiene. In total, many reaction pathways were uncovered, including the elusive stilbene hula-twist mechanism, and a previously unidentified product in butadiene dimerization. Overall, these results suggest that growing string methods provide a predictive strategy for exploring photochemistry.

Introduction

Photochemistries such as double-bond isomerization and electrocyclic reactions often pass through conical intersections (CI) on the pathways leading from initial excitation to the product state.[1–5] In these reactions, CIs act like funnels that enable ultrafast, nonradiative decay to lower-lying electronic states (**Scheme 1**). This funneling effect causes the molecule to access nuclear configurations that would otherwise be thermally disallowed, which in turn allows photochemical reactions to reach unique outcomes compared to their ground state counterparts. In a sense, CIs can be envisioned as analogous to ground state transition states (TS), where passing through these regions correspond to important reactive events. Just like TSs, CIs are not single points, but whole regions of space. These regions are called seams, and different sections of the seam can lead to qualitatively different photo products. When molecules are excited with energetic photons, the product distribution will be determined by the presence and accessibility of these seams.[6,7]

Minima on the seam, called minimum energy conical intersections (MECI), are important structures for describing photochemical reactions.[8–18] Conventional MECI and seam-space optimization algorithms, however, require extensive expert knowledge of photochemistry and CI geometries, which are far different from stable chemical structures. These techniques therefore do not easily permit the discovery of new types of photochemical reactions or simple ways to explore seam spaces. To explore complex photochemical reaction mechanisms and improve computation's ability to discover photoreactivity, new methods are required.

A few unconventional methods have proposed to enable excited-state reaction discovery. For example, this was attempted by Maeda and Morokuma with the anharmonic downward distortion following (ADDF) and the artificial-force-induced reaction (AFIR) methods, which have

been used to locate MECI.[19–25] Uncovering complete photochemical reaction mechanisms—including MECI, the seam, excited-state TS, and photoproducts—is still a challenging task, however, leaving room for new methodologies.

Research in our laboratory has made extensive use of the growing string method (GSM) to determine thermal reaction pathways and transition states (TSs) without prior knowledge of the TS structure.[26–28] In GSM, qualitative reactive coordinates such as bond additions/breaks and/or angle changes—called driving coordinates—are used to locate TSs, products, and the reaction paths connecting them. When combined with the reaction discovery tool, ZStruct,[29–31] many TSs, some unexpected, can be found at once in a parallel computation. These features would be equally useful in the context of photochemistry where MECI optimization and seam minimum energy paths are challenging to optimize.

The GSM/ZStruct strategy is herein investigated for the first time for photochemistry, where reaction pathways include CIs and seams as well as TSs and products (Scheme 1). This method includes the integration of GSM with CI optimizers, penalty function optimization, and CI topography analysis (see Theoretical Methods). To show that complex photochemical reaction spaces can be explored, photoisomerizations of ethylene and stilbene, and also butadiene dimerization are examined. Photoisomerization pathways are of interest for understanding molecular motors, molecular switches and retinal chromophores, but are notoriously challenging to study because the S_1/S_0 degeneracy persists along the torsional coordinate, leading to complex reaction mechanisms.[6] Butadiene dimerization was chosen because it can involve several modes of reaction ([2+2], [3+2], [4+2]), which, to our knowledge, has not been completely elucidated.[32,33] Overall, the results will indicate that GSM/ZStruct provides a thorough, robust and highly predictive method for identifying photochemical reaction mechanisms.

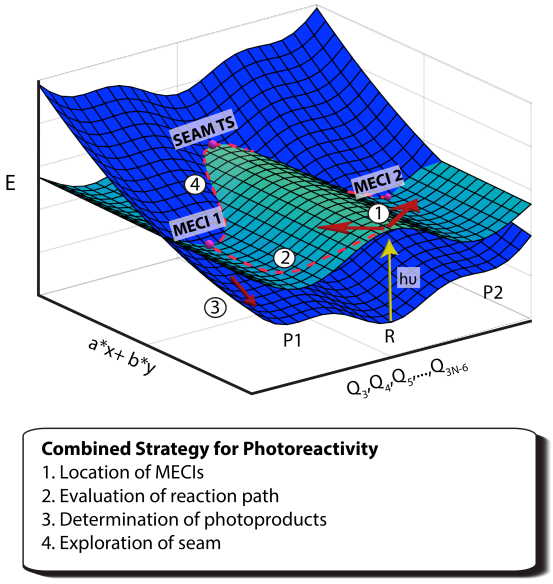

Scheme 1. Overall of photochemical reactivity search.

Background

The theory of conical-intersection-mediated photochemistry was not widely accepted until modern electronic structure theories and sufficient computational power became available,[34] whereupon Robb and coworkers developed an MECI optimization algorithm.[35] Locating MECIs has subsequently been performed using other optimizers such as the composed-step and double-Newton-Raphson algorithms.[36–40] Although there are several variants of MECI solver, these optimizers all operate by minimizing the energy gap between states and total energy simultaneously. These all require an initial starting structure that is geometrically near the MECI to be successful. This article will show that single-ended growing string method (SE-GSM) can be used to generate these structures and optimize the MECI.

Beyond MECIs, the seam[8,9,11,12,14–17,41] and non-MECI points such as seam TSs (saddle points), minimum energy path CIs,[42] and minimum distance CIs[43] are also vital components of the photochemical reaction landscape. Methods for seam optimization include seam minimum energy paths (e.g. from a seam TS),[36] constrained MECI optimization,[40,44,45] and the nudged elastic band (NEB) method which connects two MECIs.[46] GSM will also be shown capable of connecting two MECIs, and the single-ended GSM will additionally be useful for locating seams starting from just one MECI. Seam mapping with GSM is expected to be advantageous due to its lower cost compared to NEB and standard string methods,[47,48] and its ability to be easily integrated with the SE-GSM method.

MECIs and seams give key transition regions between electronic states, and further analysis can then determine the photoproducts. First, the existence or absence of TS along the reaction path from the Frank Condon region to the CI shows whether the CI is accessible. Given that the CI is accessible, the topography near the CI influences the relaxation directions to the photoproducts.[49–51] One way to find these directions is to plot the energy around the CI within the branching plane (BP), which breaks the degeneracy to first order. The BP topography can be parametrized through the CI pitch, tilt, and asymmetry.[52] Ultimately, dynamical trajectories to and from the CI dictate photoproduct yields,[5,46,53–59] and several approaches have been used to approximate such trajectories.[60,61] Such simulations, however, are highly costly, leaving room for potential energy surface analysis to map out complicated photochemical reaction pathways.

When performing analysis of seams, CIs, and photochemical reaction paths, the results will be sensitive to choice of electronic structure theory. Therefore we note that the methods used here are compatible with any electronic structure theory that treats conical intersections, gradients, and derivative couplings. For methods without derivative coupling vectors already implemented, these vectors can be approximated using the branching plane updating method,[62] or using the Davidson algorithm recently developed in our lab, which requires only standard gradients.[63]

Theoretical Methods

The CI space is a central concept for the proposed methodologies, and is defined[64] in terms of the coordinate system

$$\boldsymbol{Q} = (\boldsymbol{x}, \boldsymbol{y}, \boldsymbol{Q}_3, \boldsymbol{Q}_4, \dots, \boldsymbol{Q}_{3N-6}) \,. \qquad (1)$$

The first subspace $(\boldsymbol{x}, \boldsymbol{y})$ is called branching plane (BP), where $\boldsymbol{x}$ and $\boldsymbol{y}$ are the difference gradient and derivative coupling vectors, respectively. $\boldsymbol{x}$ and $\boldsymbol{y}$ are orthogonal to all other coordinates, $\boldsymbol{Q}_i$. At a CI, motion along $\boldsymbol{x}$ and $\boldsymbol{y}$ changes the energy gap and produces the characteristic cone shape of a CI between two electronic states. The second subspace $(\boldsymbol{Q}_3 \dots \boldsymbol{Q}_{3N-6})$ is denoted the seam space (SS) and corresponds to the 3N-8 internal coordinates which do not affect the energy gap to first order. Throughout this text, **bold font** signifies **vectors** and **matrices**.

Composed-Step Optimizer

MECI optimization reduces the SS gradient and energy gap between two electronic states to zero. Most MECI optimizers achieve this by starting with a good guess structure for the MECI, projecting out the BP contributions from the (Cartesian) gradient, and optimizing in the SS. On the other hand, one can directly construct the CI space in delocalized internal coordinates ($\boldsymbol{U}$),

which are non-redundant vectors that fully span the 3N-6 degrees of freedom within a molecular system.[26,65,66]

To form the CI subspaces, $\boldsymbol{U}$ is formed using the standard procedure,[65] and $\boldsymbol{x}$ and $\boldsymbol{y}$ (originally Cartesian vectors) are projected into the basis of internal coordinates $(\boldsymbol{U}_x, \boldsymbol{U}_y)$, but are not orthonormal. Then, the Gram-Schmidt process is applied to the set $\{(\boldsymbol{U}_x, \boldsymbol{U}_y), (\boldsymbol{U}_k; k = 1 \dots 3N-6)\}$ to produce the orthonormal vectors

$$\boldsymbol{V} = \{(\boldsymbol{U}_x, \boldsymbol{V}_y), (\boldsymbol{V}_k; k = 3,4,5 \dots 3N-6)\} \qquad (2)$$

where the first two vectors represent the BP, orthonormalized with respect to $\boldsymbol{U}_x$, and the $\boldsymbol{V}_k$ vectors define the SS.

With these vectors, the composed-step optimizer (Scheme 2)[36,38] consists of two component, the first

$$\Delta \boldsymbol{v}_x = -\frac{\Delta E}{|\boldsymbol{g}_x|}\boldsymbol{U}_x \qquad (3)$$

moves the geometry closer to the CI, where ΔE is the energy gap between the upper and lower surfaces and $|\boldsymbol{g}_x|$ is the magnitude of the difference gradient. The second component minimizes the total energy by an eigenvector optimization in the seam-space:

$$\Delta \widetilde{\boldsymbol{v}}_{SS,i} = -\frac{\widetilde{\boldsymbol{g}}_i}{\widetilde{\boldsymbol{H}}_{ii}+\boldsymbol{\lambda}}\widetilde{\boldsymbol{V}}_{SS,i} \qquad (4)$$

where $\widetilde{\boldsymbol{V}}_{SS,i}$ and $\widetilde{\boldsymbol{H}}_{ii}$ are the eigenvectors and eigenvalues of the seam-space Hessian, respectively, $\widetilde{\boldsymbol{g}}_i$ is the average gradient, and λ a shift factor. After back-transforming equation 4 to the CI basis ($\boldsymbol{V}$), the optimization step is composed of equations 3 and 4:

$$\Delta \boldsymbol{v} = \Delta \boldsymbol{v}_x + \Delta \boldsymbol{v}_{SS} \qquad (5)$$

These steps are taken until the MECI is reached.

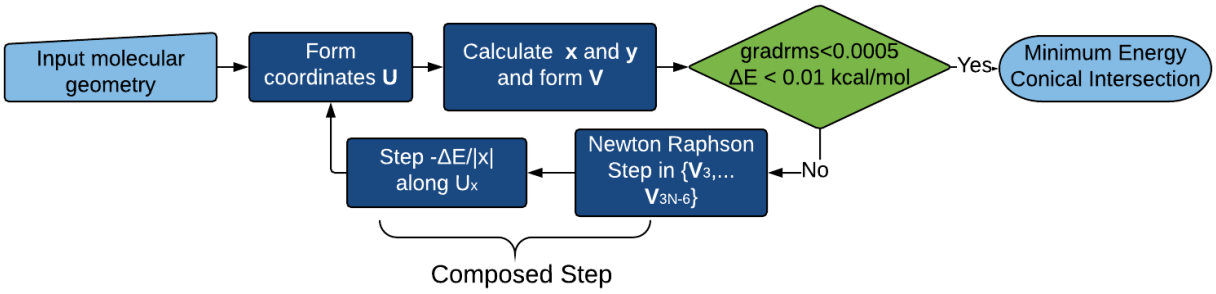

Scheme 2. Composed-step optimizer in delocalized internal coordinates. Each cycle of the optimizer takes a composed step until the gradient and energy gap are converged.

Locating MECI with GSM

GSM develops a reaction path by iteratively adding and optimizing discrete structures, called nodes, along a specified reaction tangent,[26,28] and herein will be shown to be useful for locating MECIs starting far from the seam space. Figure S2 of the supporting information details the key steps of the GSM algorithm. The reaction tangent of GSM is defined using the standard delocalized internal coordinates ($\boldsymbol{U}$) as

$$\boldsymbol{U}_c = \sum_{k=1}^{3N-6}(\Delta \boldsymbol{q}^p|\boldsymbol{U}_k)\boldsymbol{U}_k \qquad (6)$$

where $\Delta \boldsymbol{q}^p$ is the specified change in primitive internal coordinates ($\boldsymbol{q}$) describing the reaction. These vectors, called driving coordinates, allow GSM to explore in a specific direction (e.g. by the arrows of Scheme 1) using the coordinate system

$$\boldsymbol{V}^* = \{(\boldsymbol{U}_c), (\boldsymbol{V}_k^*; k = 2,3,4 \ldots 3N-6)\} \qquad (7)$$

where coordinates $\boldsymbol{V}_{\boldsymbol{k}}^*$ are orthogonal to $\boldsymbol{U}_c$.

To locate an MECI, single-ended GSM moves along $\boldsymbol{U}_c$ and optimizes in all orthogonal directions on the energy surface[43] defined by

$$E(\boldsymbol{V}^*) = \bar{E}_{ij}(\boldsymbol{V}^*) + \sigma \frac{\Delta E_{ij}(\boldsymbol{V}^*)^2}{\Delta E_{ij}(\boldsymbol{V}^*)+\alpha} \qquad (8)$$

where $\bar{E}_{ij}$ is the average energy, σ and α are penalty parameters, and ΔE_{ij} is the energy gap. This strategy therefore permits a simultaneous search and optimization to the nearest conical intersection in the search direction. Once the frontier node of GSM gets close to a CI, the composed step optimizer fully refines the MECI. The computational details section describes the criteria for switching between driving and optimization steps.

Seam Space GSM

The seams connecting MECIs will be mapped using GSM as well. This procedure combines the tangent vector (defined using eqn 6) with the two BP vectors in a coordinate system

$$\boldsymbol{V}' = \{(\boldsymbol{U}_c), (\boldsymbol{V}_x, \boldsymbol{V}_y), (\boldsymbol{V}_k; k = 4,5,6 \ldots 3N-6)\}. \qquad (9)$$

As before, the Gram-Schmidt process is applied to produce a nonredundant, orthonormal set, $\boldsymbol{V}'$, with 3N-6 total degrees of freedom. All vectors are orthonormalized with respect to $\boldsymbol{U}_c$ to preserve the direction of $\boldsymbol{U}_c$. This means that $\boldsymbol{U}_c$ will typically overlap with the original BP until the path converges fully to the seam, and in practice this choice results in stable optimization. Node optimization is performed using the composed-step algorithm in the unconstrained part (3N-7 dimensions) of the coordinate space (Scheme 3).

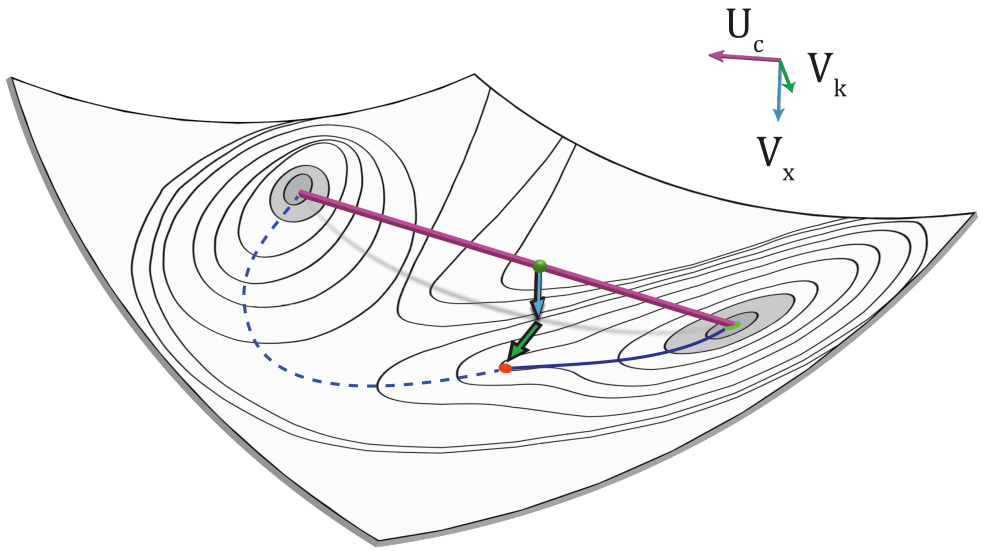

Scheme 3. Multidimensional representation that shows the operation of the growing string method seam mapping. Curved contour plot is the seam space (3N-8 dimensional) represented in the full molecular space (3N-6 dimensions). Minima on the contour plot are minimum energy conical intersections. Purple line is the tangent constraint vector ($\mathbf{U_c}$). A composed step along along ($\mathbf{V_x}$) and ($\mathbf{V_k}$; k=4,5,6,…,3N-6) is required to optimize the minimum energy seam path (dashed line).

This coordinate system enables two modes of operation for seam optimization in GSM. First, double-ended GSM is available to connect pairs of MECIs, by growing inward and adding additional nodes until the string connects. Alternatively, a single-ended search starting from one MECI can explore via driving coordinates, permitting a search along a seam for a second MECI. After the full string is formed with either method, full optimization of the seam in the coordinate system of equation 9 is performed, providing a minimum energy path along the seam (Scheme 3).

Determining photoproducts

Photoproduct determination and optimization is initialized by taking small displacements (0.1 Å) in the BP, based on a cross-section analysis defined in polar coordinates as[52]

$$E(r,\theta) = E^{MECI} + \delta_{gh}\left(\sigma\cos(\theta-\theta_s) - \sqrt{1+\Delta_{gh}\cos 2\theta}\right) \quad (10)$$

where δ_{gh} is the pitch, θ_s is the tilt heading, and Δ_{gh} is the asymmetry. These parameters can be calculated given $\boldsymbol{x}, \boldsymbol{y}$ and the average energy gradient. Because the BP vectors can be interchanged at a CI through rotation of the electronic states, $\boldsymbol{x}, \boldsymbol{y}$ are chosen such that Δ_{gh}>0 and $0 < \theta_s < \frac{\pi}{2}$.

Displacements in the direction of the minima and maxima of equation 10 are chosen as starting pathways to photoproducts. Optimization from the minima is analogous to the minimum energy pathways proceeding downhill from the CI, whereas optimization from the maxima in the cross-section are also investigated because they sometimes lead to minima not in the immediate vicinity of the CI cross-section.[49] Therefore, photoproduct optimization can be initialized given the BP vectors, and the sensitivity of the decay channels to the topography (e.g. minimum versus maximum) will be captured by sampling of both types of pathways.

Computational Details:

GSM methods are implemented in C++, and will be made available online on Github.[67] The Hessian is formed at each step of the optimization, from the Hessian in primitive coordinates

$$\boldsymbol{H} = \boldsymbol{U}^{T\prime}\boldsymbol{H}^{p}\boldsymbol{U}' \quad (11)$$

but only the non-constrained seam space coordinates are diagonalized and used in the Newton-Raphson optimization. The Broyden−Fletcher−Goldfarb−Shanno (BFGS) method is used to update a diagonal initial Hessian in primitive coordinates, which is transformed into a delocalized internal coordinate Hessian at each step.[68–71] The MECI is considered converged when the energy gap between the two states is less than 0.01 kcal mol^{-1} and the seam-space root-mean-squared (RMS) average gradient is less than 0.0005 Ha/Å. For seam mapping the calculation terminates when all the nodes are converged to within a predefined threshold or the total gradient is below a predefined threshold that is dependent on the system size and number of nodes. Each node is considered converged when the energy gap between the two states is less than 1.0 kcal mol^{-1} and the gradient is converged to 0.0025 Ha/Å. The total gradient convergence criterion was chosen to be $(M-2) * 0.0025 * \sqrt{3N-6}$, where M is the number of GSM nodes.

Knowing where to stop the SE-GSM algorithm and initiate the composed step optimizer is an important criterion for the successful location of MECI. Since SE-GSM should be generally moving closer to the CI—not further away—string growth terminates when ΔE_{ij} increases at the frontier node. Alternatively, if the string reaches the "product" specified by $\Delta\mathbf{q}$ (eqn 6), this indicates that

no further growth of the string is possible, and the composed step optimizer is turned on immediately.

MECI SE-GSM calculations employed a maximum of 5 iterations per node, and a maximum growth step size (dqmax) of 0.4 Å-radians. Larger dqmax generally decreases the number of nodes in a calculation and therefore decreases the number of total gradients. In the small systems investigated here, however, a small dqmax is beneficial for MECI optimization because the final node is usually closer to the seam. The last node before MECI optimization is optimized for at most 60 steps, or until converged within 0.001 Ha/Å. The penalty function optimizer utilized σ as 1.0, for all nodes except for the final guess node, which is optimized using σ as 3.5. Staggering σ from small to large helps SE-GSM correctly find the desired MECI.

Seam mapping GSM calculations employed 3-5 optimization iterations per node per cycle, and dqmax values from 0.2 to 0.8 Å-radians. The optimization success is sensitive to these parameters and string growth should be monitored. In general, a smaller dqmax should be used for small molecules and/or short seam paths to ensure a refined reaction pathway.

The ZStruct method generates driving coordinates consisting of add and break coordination changes between reactive atoms. This is usually subject to the constraint that the driving coordinate can have up to two adds and one break, and the coordination of the atoms doesn't exceed a maximum and minimum coordination number.[30] In this work, however, add connection moves are used exclusively, leading to N^4 scaling in the number of generated driving coordinates, where N is the number of reactive atoms.

The methods invoke MOLPRO CASSCF to provide the quantum mechanical energies, gradients and derivative coupling vectors.[72] Active space selection was performed by considering the electrons involved in the excitation and reaction coordinate. Active space choices are listed in the figures below.

Results and Discussion

Exploratory via SE-GSM

In many photoreactions the qualitative reaction coordinates are known but not precisely quantified. For example, in the photoisomerization of ethylene the qualitative reaction coordinate is double bond torsion, but the CI also introduces pyramidalization of the carbon. SE-GSM captures this behavior by adding nodes along a driving coordinate (torsion) and optimizing in orthogonal directions (pyramidalization). Therefore SE-GSM identifies and follows directions to MECI that are not necessarily specified prior to the search. Importantly, different MECI within the same reactive system can be found by sampling a variety of driving coordinates. To show the capabilities of these methods, photoisomerization pathways for ethylene and stilbene are investigated as the initial test cases.

Ethylene Conical intersections

The well-known twisted-pyramidalized (also called H-bridging[73]) and ethylidene-like MECIs between S_0 and S_1 are reproduced here using SE-GSM (Figure 1).[74] While both MECIs were found by driving a torsional coordinate, the second case also used two driving coordinates, one of which specified H-atom transfer (Table 1).

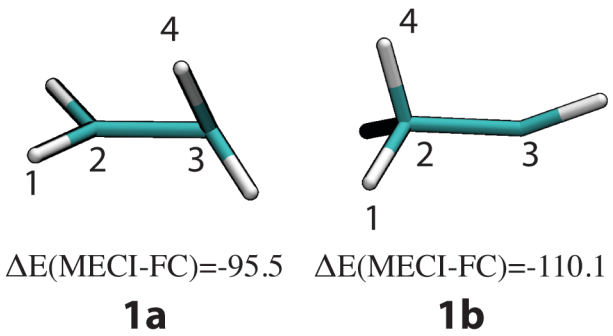

Figure 1. Ethylene minimum energy conical intersections calculated using CAS(4,4)/6-31G* with SE-GSM. Energy is reported in kcal/mol with respect to Franck-Condon point. Paths to the MECI are barrierless.[60]. Atom numbers in figure are driving coordinate indices (see Table 1).

Performance metrics for SE-GSM with these two MECI are reported in Table 1. Driving cycles represent the computational costs (eqn 8) of generating the MECI guess structures. Once this initial structure is found, the MECI optimization quickly reaches accurate MECIs because the RMS distance from the guess to the true MECI is small, under 0.07 Å. Compared to a standard MECI optimizer in Molpro,[35] the final geometries agree well (to within 0.01 Å RMS) and the energies to within 0.05 kcal/mol. These examples demonstrate that the SE-GSM process for MECI optimization provides reasonable results for ethylene, at computational costs of less than 100 gradients for each MECI.

Table 1. Ethylene MECI Results from SE-GSM, compared to standard optimizers.

MECI	Driving Coordinates[a]	Driving Cycles	MECI Cycles	Guess to MECI Distance (RMSD Å)[b]	Calc. MECI vs. Ref. MECI, (RMSD Å)[c]	Calc. E(MECI) – Ref. E(MECI) (kcal/mol)[c]
1a	TORSION(1,2,3,4) = 90	56	10	0.0611	0.0011	0.01
1b	TORSION(1,2,3,4)=120, ADD(4,2), BREAK(3,4)	55	39	0.0658	0.0076	-0.03

[a] TORSION(1,2,3,4)=90, refers to a driving coordinate to push angle 1-2-3-4 towards 90 degrees, starting from its current position. [b] root-mean squared distance in Å from penalty optimized structure to composed-step (CS) optimized MECI. [c] root-mean squared distance in Å from composed-step (CS) optimized MECI to MECI from MOLPRO, see computational details.

Three seam reaction pathways and corresponding TSs were found for the ethylene system using the GSM seam optimization approach, and these are reported in Figure 2. Among these three, a tilted seam TS (**2a**) between **1a** and **1b** has been previously reported and is reproduced here.[46] **2a** can be found using 7 or 9 GSM nodes and has energy relative to the FC point of -66.5 kcal/mol. A second, unexpected low energy seam TS was also found between **1a** and **1b,** which occurs along a roaming atom reaction pathway (**2b**).[21,75] Seam TS **2b** was found using 11 or 13 GSM nodes, and has energy relative to the FC point of -84.5 kcal/mol. Two seam TSs were located (using the same string endpoints) due to a difference in step size during GSM growth, with 7 nodes having a larger step size than 11 nodes. Interestingly, GSM is able to locate the two paths of this bifurcating potential energy surface, a “long” path and a “short” path, by just adjusting the step size during string growth. Lastly, a seam TS **2c** between tilt isomers of **1a** has been reported[46] and is reproduced here. This conical intersection is distinguished by a pyramidalized,

but not tilted methylene group. Seam TS **2c** was found using 11 GSM nodes, and has an energy relative to the FC point of -84.1 kcal/mol.

The tests on the ethylene system demonstrate that GSM has significant exploratory ability, providing not only the CI structures that are previously known, but an additional seam-space TS that has not been reported. The tests that follow will affirm these initial indications.

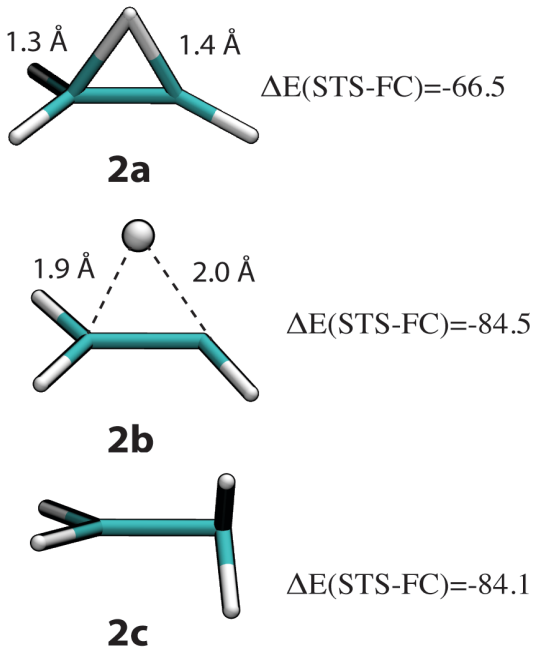

Figure 2. Ethylene seam TS (STS) calculated using CAS(4,4)SCF/6-31G* with DE-GSM. Energies in kcal/mol with respect to the Franck-Condon point.

Stilbene Conical Intersections

Compared to ethylene, stilbene has additional available photoreaction pathways due to the asymmetry around its central double bond. Stilbene is most stable in the *trans* conformation but can isomerize after absorption of a photon to *cis* via one-bond flip, *cis* via hula-twist, or ring-close to dihydrophenanthrene (DHP). The hula twist mechanism, which preserves the relative position of the phenyl groups has been hypothesized as favored for *cis*-*trans* isomerization in constrained media, as this mechanism reasonably preserves the molecular volume.[73,76,77]

For stilbene, *cis*-kinked (twisted pyramidalized[78]) and DHP-like MECI have been reported.[79] For related polyene systems, such as butadiene and hexatriene, additional CIs have been found such as *cis*-kinked diene, *trans*-kinked diene and H/vinyl (H-bridging) MECI, as well as seam saddle points hypothesized to be responsible for the hula-twist mechanism.[80] Analogies for all of these structures were found for stilbene using SE-GSM starting from a *trans* geometry. The driving coordinates and structures are shown Table 2 and Figure 3, respectively.

In total, five MECI (**3a**-**3e**) and one seam TS (**3f**) were located using SE-GSM (Figure 3). Additional seam TSs for the tilt seam coordinate (between **3a** and **3c**) and hydrogen transfer coordinate (between **3c** and **3d**) were found using DE-GSM (see Supporting Information). **3a** and **3c** are *cis*-kinked MECI analogous to twisted-pyramidalized MECI **1a**, but differ from each other by the tilt of their phenyl ring with respect to the central double bond. **3b** is the trans-kinked MECI related to CIs in polyenes,[80] and was found by a one-bond flip of the central double bond. **3d** is analogous to the ethylidene-like conical intersection **1b** and leads to a reactive carbene intermediate or *cis*- and *trans*-stilbene. **3e** is the DHP-like MECI which can ring-close to DHP. Lastly, **3f** is related to the volume conserving hula-twist CI reported by Houk et al for dienes,[80] and was found using SE-GSM by rotation of the phenyl ring in **3c**. **3a** and **3e** agree with structures reported in the literature.[78,79] To our knowledge **3b**-**3d** and **3f** have not been reported for stilbene, but they do resemble conical intersection geometries in dienes.[73,80]

Thus, a wide range of tilt and dihedral angles as well as degree of hydrogen bond transfer are present in the MECI and seam TSs, and these lead to different reaction possibilities. As can be

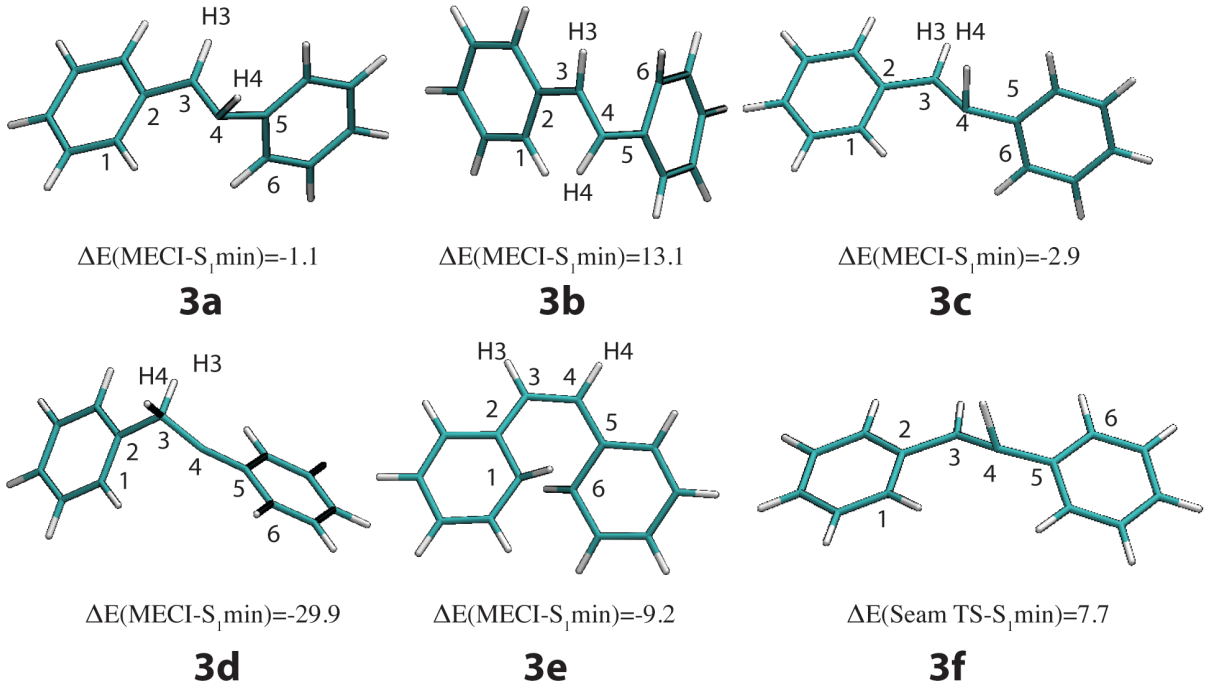

Figure 3. Stilbene conical intersections calculated using CAS(2,2)SCF/6-31G with SE-GSM. Energies in kcal/mol with respect to the S_1 minimum. Atom numbers are driving coordinate indices (see Table 2).

seen in the CI structures, **3a**-**3c** flip the orientation of the phenyl groups (i.e. atoms 1 and 6 will land on the same side), whereas **3f** preserves the relative orientation of the phenyl groups with respect to each other. Therefore, **3a-3c** are important for the one-bond flip mechanism, and **3f** is predicted to be important for the hula-twist mechanism.

Importantly, a comparison of the driving coordinates (which are qualitative) to the (quantitative) dihedral angles of the MECIs (Figure 3) shows that prior quantitative details of these MECI geometries are unnecessary for their optimization via SE-GSM. Instead, the driving coordinates take the Franck-Condon initial geometry, perturb it in the direction of each of these MECIs, and thus permit facile discovery of all 5 MECIs *from the same starting structure*. Together with the results from ethylene, the stilbene simulations demonstrate that GSM is effective at optimizing MECIs and seam-space reaction pathways. In the next section, a more complex photoreaction will be studied to show the full power of MECI exploration using GSM.

Table 2. Stilbene MECI results from SE-GSM.

Minimum Energy Conical Intersection	Driving Coordinates	Driving Cycles	MECI cycles	ϕ(2,3,4,5)	ϕ(H3,2,3,H4)	ϕ(3,4,5,6)
3a	TORSION(2,3,4,5)=90, TORSION(H3,3,4,H4)=0	83	25	114.3	41.5	-98.1
3b	TORSION(2,3,4,5)=90	81	20	93.9	140.9	36.3

3c	TORSION(2,3,4,5)=180, TORSION(H3,3,4 H4)=90	77	41	146.6	61.1	-53.1
3d	TORSION(2,3,4,5)=120, ADD(H4,3), BREAK(H4,4)	95	18	84.5	114.4	179.4
3e	TORSION(H3,3,4,H4)=0, TORSION(2,3,4,5)= 0, ADD(1,6)	119	11	21.4	16.7	10.7
3f[a]	TORSION(3,4,5,6)=-50	-	-	137.9	71.1	47.9

[a]Seam transition state found from MECI **3c.**

Butadiene dimerization reaction discovery

Photochemical reactions with changes in covalent bonding are key challenges for simulation. In this space, reaction path discovery is possible with SE-GSM using driving coordinates that are systematically generated to sample many possible changes in bonding. To do this, the ZStruct reaction discovery method[29–31] is used to combinatorially sample search directions based on bond addition and breaking coordinates, where SE-GSM completes the MECI optimizations. ZStruct has seen extensive use in ground-state reactions,[81–87] and is applied here for the first time to photo-induced reactivity.

As a challenging test case, the dimerization of butadiene is studied[32,33] as a complex photoreaction with many product channels. Under direct UV irradiation, butadiene has been observed to form 50% 2-vinylbicyclo[3.1.0]hexane and/or 3-vinylbicyclo[3.1.0]hexane (I), 30% 1,2-divinylcyclobutane (II), and 8% cycloocta-1,5-diene (III). A fourth species accounting for the remaining product (~10%) was unidentified. While 1,3-divinylcyclobutane was not mentioned in the original study, it is possible that this was not separated from 1,2-divinylcyclobutane. Interestingly, this product distribution is markedly different than seen in triplet sensitization and thermal reactions. For example, 4-vinylcyclohex-1-ene (V) is a major product in triplet-sensitized reactions of butadiene and has also been observed in the thermal dimerization but does not appear in the UV chemistry. This diversity of products provides a great opportunity for reaction discovery simulations to provide details about the photoproduct generation mechanisms and corresponding CI space.

SE-GSM and ZStruct method were applied to a pair of *cis*-butadiene molecules, which were promoted to their lowest energy excited state. ZStruct generated 120 combinations of driving coordinates for the dimerization reaction, considering all carbon, but not hydrogen, as reactive. Of these combinations, 37 produced unique MECI based upon root-mean-squared distances and coordinate connectivity metrics.

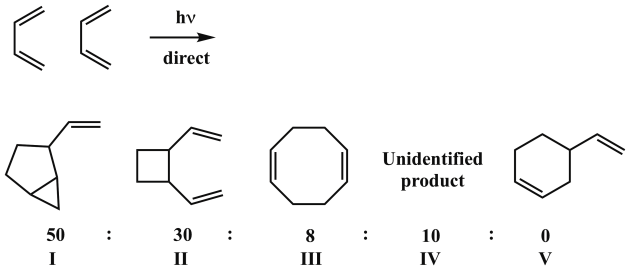

Scheme 4. Experimental photoproduct distributions from ref. [42].

Because existence of an MECI does not guarantee its accessibility, multiple reaction paths to each MECI were considered, starting from the handful of local minima of the excited state surface

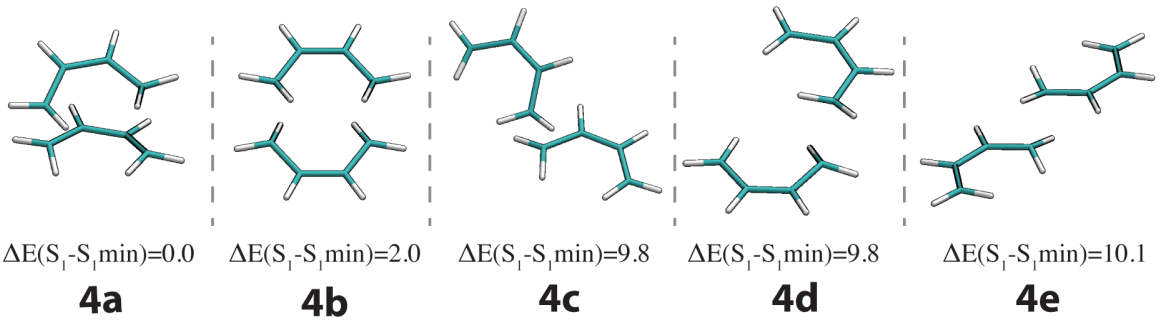

Figure 4. Optimized geometries for S_1 minima located with CAS(8,8)SCF/6-31G* from aligned ZStruct structures. Energies in kcal/mol with respect to the global S_1 minimum, structure **4a**.

near the Franck-Condon points. From the initial ZStruct-aligned structures, five excited-state minima were located (Figure 4). S_1 minima **4a** and **4b** are tetraradicaloid and the lowest in energy. **4b** is related to the so-called pericyclic minimum.[33] **4c**-**4e** minima have one radical from each molecule interacting with the other.

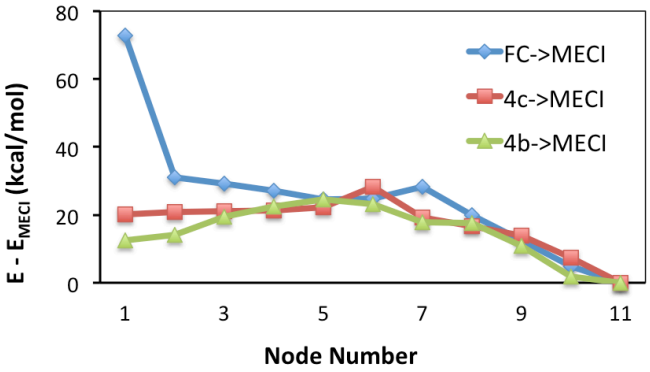

Figure 5. Reaction path analysis reveals that excited-state barrier depends on the binding of the dimers before reaching the MECI. Reaction paths were computed using DE-GSM with CAS (8,8)SCF/6-31G*. The FC point is the aligned, but unoptimized planar monomers.

The reaction paths from the lower energy intermediates, **4a** and **4b**, typically result in higher activation energies to reach the MECIs, compared to **4c**-**4e**. A typical case is shown in Figure 5. From **4b** to the 5-coordinate MECI (**c-1** in Supporting Information), the reaction path has an activation barrier of 12.0 kcal/mol, which is in agreement with previous results calculated using CAS(4,4)SCF/4-31G.[33] The pathway, in contrast, is largely downhill from **4c**, with a small barrier of 7.8 kcal/mol. A similar effect is found in other pathways to reach the various MECI (see reaction pathways in SI section 3).

From the accessible MECI, photoproducts were optimized from the minima and maxima of the MECI branching plane cross-sections. In total, 12 energetically accessible constitutional isomers and their diastereomers were identified (Figure 6). Additional photoproducts were also identified but are not accessible due to having high energy MECI or large excited state activation barriers with respect to the S_1 local minima.

All experimentally observed photoproducts, (I), (II), and (III) have at least one low energy pathway, as well as additional, higher energy pathways arising from differences in S_1 minima, MECI or stereochemistry. Diastereomers of (I) form from a [3+2] cycloaddition, which upon ring-closing form an unstable methylene. The methylene carbon promptly ring-closes to form the resulting three-membered ring (see Figure 7). If the methylene and vinyl group are on the opposite sides of the 5-membered ring, then (1S,2R,5R)-(I) or (1S,2S,5R)-(1) forms. When these groups are on same side, (1R,3s,5S)-(I) or (1R,3r,5S)-(I) forms. 4-vinylcyclohex-1-ene (V) also

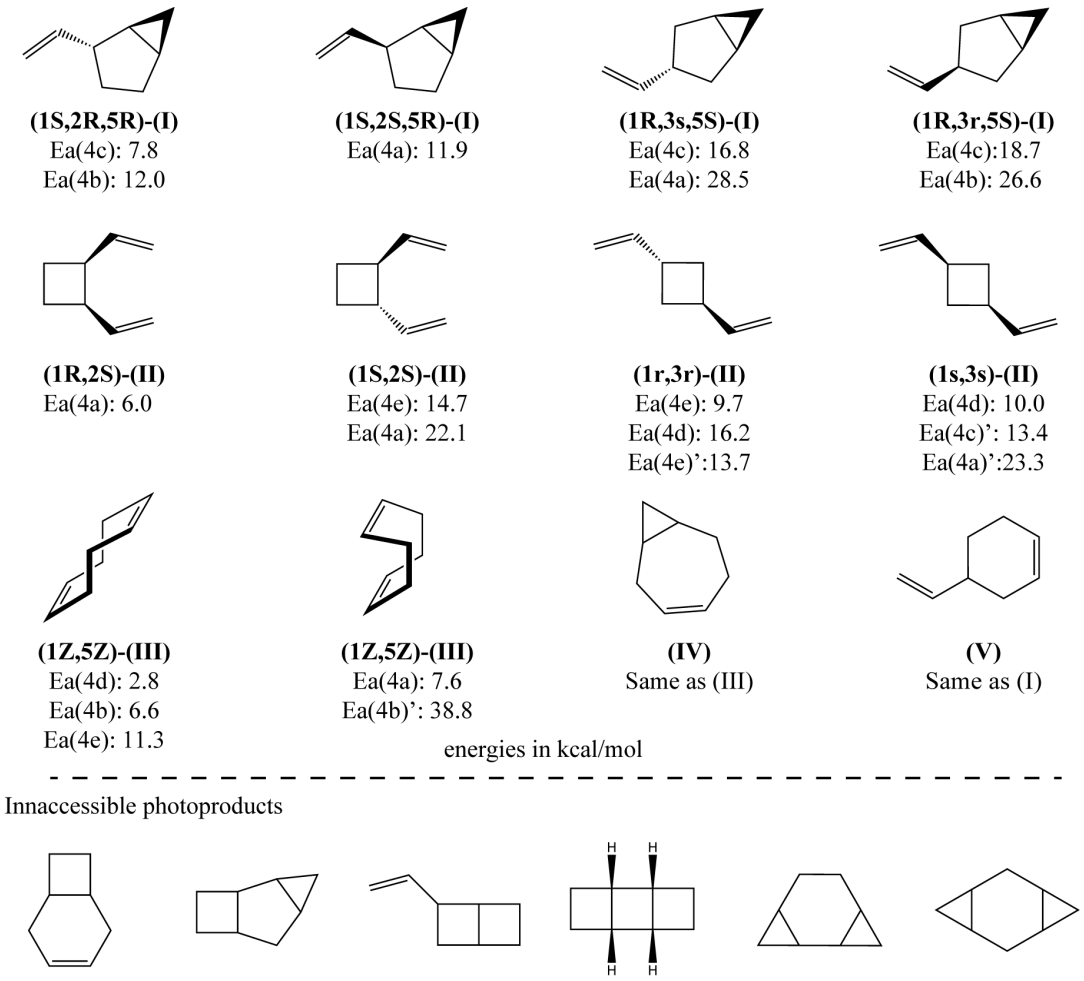

Figure 6. Reaction products discovered using combinatorial reactive hypothesis generator ZStruct and single-ended GSM. Activation energies are in kcal/mol with respect to the labeled local minima. Ea' correspond to different MECI leading to the same product. Inaccessible products due to large reaction pathway barriers and high MECI energies.

arises from all MECI leading to the diastereomers of (I) and therefore is produced from the same reaction pathways. (V) forms, however, from different initial directions leading away from the MECI funnel. Diastereomers of (II) form from rhomboidal [2+2] cycloaddition MECI which agree with previously reported MECI.[33] The boat and chair conformations of cyclo-1,5-octadiene (III) arise from [4+4] cycloaddition MECI close to the initial geometries of **4a** and **4b**. Bicyclo[5.1.0]oct-3-ene forms from the same MECI of (III) along different initial relaxation coordinates. Based on the results in Figure 6, the unidentified dimer (IV) from experiment is likely bicyclo[5.1.0]oct-3-ene, which shares the same conical intersection as (III), and has similar yield (~10 %).

These results are largely in agreement with available experimental results, but lead to an important question: why are there energetically accessible 4-vinylcyclohex-1-ene (V) pathways, but this species is not observed in experiment? A possible explanation comes from a reaction path to the MECI that gives (V) and (I)-(1R,3r,5S), which contains a nearby extended seam (Figure 7a). The first accessible CI along this seam is a minimum distance conical intersection (MDCI),[43] which would be the first CI approached along this path starting from the S1 minimum.

The photoproducts of this (V)/(I) reaction path are shown in Figure 7b. (I)-(1R,3r,5S) arises from the maxima of the MECI cross-section, and (V) from the minima. In the latter case, the biradical recouples in a [4+2] arrangement. At the MDCI, which considerably differs in bond length **A** from the MECI, forms (I) or returns to the reactant structure without producing photoproduct. The MDCI can revert to reactants because carbon-carbon bond **A** has not yet been formed and therefore the geometry does not recouple to form (V). Thus, we hypothesize that decay at the MDCI, rather than the MECI, prevents the formation of (V).

In arene-alkene cycloaddition, the seam TS connecting [3+2] cycloaddition MECI has been hypothesized to be responsible for para ([4+2]) selectivity.[10] In butadiene dimerization, however, it is possible that the seam contains high energy points that prevent [4+2] dimerization (Figure 7b). Therefore, to provide additional insight**,** a SE-GSM seam calculation was performed (Figure 7c) from the MECI in Figure 7a using a breaking carbon-carbon bond **A** and a forming carbon-carbon bond **B** as driving coordinates. The SE-GSM seam method was necessary since the [3+2] MECI with carbon-carbon bond **A** was not found in the MECI search using ZStruct, and therefore no DE-GSM seam could be optimized. Notably, unlike the seam in arene-alkene cycloaddition that contains a low-lying seam TS and MECI along this coordinate,[10] no such TS or MECI was located, which is consistent with the SE-GSM and ZStruct findings. Thus, the seam landscape is significantly different from the arene-alkene cycloaddition and may be the source of the difference in reactivity. Future studies including dynamics will be valuable to better investigate how the extended seam affects photoproduct distributions.

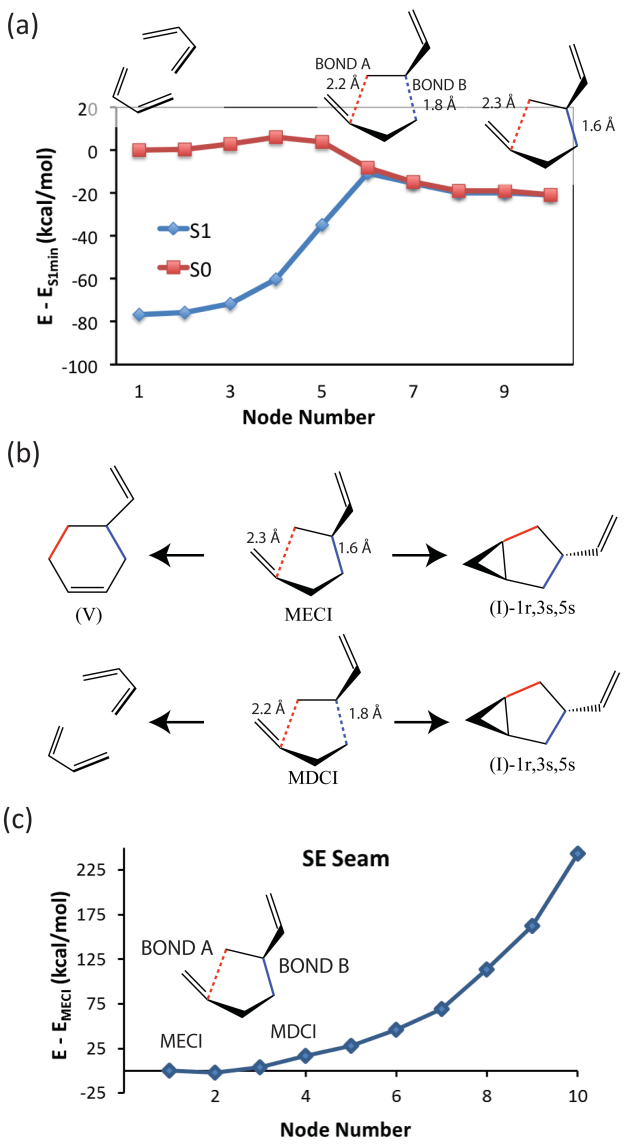

Figure 7. (**a**) Reaction path from **4c** to MECI leading to (I)-1r,3s,5s and (V) products that shows ground and excited-state merging to form a seam and a minimum distance CI (MDCI) (**b**) photoproducts from the minimum and maximum of the CI branching plane cross-section for the MECI and MDCI (**c**) SE-GSM seam using breaking bond A and adding bond B driving coordinate.

Conclusions

The growing string method is a powerful tool for reaction path optimization, and this tool has been herein enabled to search for conical intersections and seam space reaction pathways. These methods provide a useful platform for studying photochemical reactions and have the important

distinction of being useful even when little prior knowledge of the photochemical reaction pathways is available.

GSM located new excited state reaction pathways even in the well-understood ethylene and stilbene isomerization reactions. In addition, a combination of GSM with ZStruct was able to systematically explore reaction possibilities for the photodimerization of butadiene. The major, experimental photoproducts were found in the set of computed, energetically accessible products. The unidentified product in the experiment is likely bicyclo[5.1.0]oct-3-ene, since it shares the same conical intersection as cycloocta-1,5-diene and has similar yield. Interestingly, a non-stationary point on the seam, explored using GSM, is found to be important in the formation (or lack thereof) of 4-vinylcyclohex-1-ene. We anticipate that continued applications of the ZStruct/GSM combination will be useful to map CI spaces in emerging, complex photoreactions.

Acknowledgements
Support for this project was provided by the National Science Foundation through CHE-1551994.

References

1 M. Klessinger, Theoretical models for the selectivity of organic singlet and triplet photoreactions, *Pure Appl. Chem.*, 1997, **69**, 773–778.
2 M. A. Robb, F. Bernardi and M. Olivucci, Conical intersections as a mechanistic feature of organic photochemistry, *Pure Appl. Chem.*, 1995, **67**, 783–789.
3 B. G. Levine, T. J. Mart and T. J. Martínez, Isomerization through conical intersections., *Annu. Rev. Phys. Chem.*, 2007, **58**, 613–634.
4 M. Boggio-pasqua, *Computational mechanistic photochemistry : The central role of conical intersections*, Universite Toulouse III <tel-01184241>, 2015.
5 A. Kazaryan, J. C. M. Kistemaker, L. V Schafer, W. R. Browne, B. L. Feringa and M. Filatov, Understanding the dynamics behind the photoisomerization of a light-driven fluorene molecular rotary motor., *J. Phys. Chem. A*, 2010, **114**, 5058–5067.
6 I. Schapiro, F. Melaccio, E. N. Laricheva and M. Olivucci, Using the computer to understand the chemistry of conical intersections., *Photochem. Photobiol. Sci.*, 2011, **10**, 867–886.
7 L. Blancafort, Photochemistry and Photophysics at Extended Seams of Conical Intersection, *ChemPhysChem*, 2014, 3166–3181.
8 B. F. E. Curchod, A. Sisto and T. J. Martínez, Ab Initio Multiple Spawning Photochemical Dynamics of DMABN Using GPUs, *J. Phys. Chem. A*, 2017, **121**, 265–276.
9 M. J. Paterson, M. a. Robb, L. Blancafort and A. D. DeBellis, Mechanism of an exceptional class of photostabilizers: A seam of conical intersection parallel to excited state intramolecular proton transfer (ESIPT) in o-hydroxyphenyl-(1,3,5)-triazine, *J. Phys. Chem. A*, 2005, **109**, 7527–7537.
10 J. J. Serrano-Pérez, F. De Vleeschouwer, F. De Proft, D. Mendive-Tapia, M. J. Bearpark and M. a. Robb, How the conical intersection seam controls chemical selectivity in the photocycloaddition of ethylene and benzene, *J. Org. Chem.*, 2013, **78**, 1874–1886.
11 M. Reguero, M. Boggio-pasqua and M. a Robb, Intramolecular Charge Transfer in 4-Aminobenzonitriles Does Not Necessarily Need the Twist, *J. Am. Chem. Soc.*, 2005, **127**, 315–318.
12 I. Gómez, M. Reguero and M. A. Robb, Efficient photochemical merocyanine-to-spiropyran

ring closure mechanism through an extended conical intersection seam. A model CASSCF/CASPT2 study, *J. Phys. Chem. A*, 2006, **110**, 3986–3991.

13 M. Kobyłecka, A. Migani, D. Asturiol, J. Rak and L. Blancafort, Benign Decay vs. Photolysis in the Photophysics and Photochemistry of 5-Bromouracil. A Computational Study, *J. Phys. Chem. A*, 2009, **113**, 5489–5495.

14 M. Boggio-Pasqua, M. J. Bearpark, P. A. Hunt and M. A. Robb, Dihydroazulene/vinylheptafulvene photochromism: A model for one-way photochemistry via a conical intersection, *J. Am. Chem. Soc.*, 2002, **124**, 1456–1470.

15 M. Boggio-Pasqua, M. Ravaglia, M. J. Bearpark, M. Garavelli and M. a. Robb, Can Diarylethene Photochromism be Explained by a Reaction Path Alone? A CASSCF Study with Model MMVB Dynamics, *J. Phys. Chem. A*, 2003, **107**, 11139–11152.

16 A. Migani, L. Blancafort, M. A. Robb and A. D. DeBellis, An extended conical intersection seam associated with a manifold of decay paths: Excited-state intramolecular proton transfer in O-hydroxybenzaldehyde, *J. Am. Chem. Soc.*, 2008, **130**, 6932–6933.

17 M. Garavelli, C. S. Page, P. Celani, M. Olivucci, W. E. Schmid, S. A. Trushin and W. Fuss, Reaction Path of a sub-200 fs Photochemical Electrocyclic Reaction, *J. Phys. Chem. A*, 2001, **105**, 4458.

18 J. D. Coe, M. T. Ong, B. G. Levine and T. J. Martínez, On the extent and connectivity of conical intersection seams and the effects of three-state intersections, *J. Phys. Chem. A*, 2008, **112**, 12559–12567.

19 S. Maeda, K. Ohno and K. Morokuma, Exploring multiple potential energy surfaces: Photochemistry of small carbonyl compounds, *Adv. Phys. Chem.*, , DOI:10.1155/2012/268124.

20 Y. Harabuchi, S. Maeda, T. Taketsugu, N. Minezawa and K. Morokuma, Automated Search for Minimum Energy Conical Intersection Geometries between the Lowest Two Singlet States S 0 / S 1 - MECIs by the Spin-Flip TDDFT Method.

21 S. Maeda, T. Taketsugu, K. Ohno and K. Morokuma, From Roaming Atoms to Hopping Surfaces: Mapping out Global Reaction Routes in Photochemistry, *J. Am. Chem. Soc.*, 2015, 150223131927005.

22 Y. Harabuchi, T. Taketsugu and S. Maeda, Exploration of minimum energy conical intersection structures of small polycyclic aromatic hydrocarbons: toward an understanding of the size dependence of fluorescence quantum yields., *Phys. Chem. Chem. Phys.*, 2015, **17**, 22561–22565.

23 S. Maeda, T. Taketsugu and K. Morokuma, Exploring Pathways of Photoaddition Reactions by Artificial Force Induced Reaction Method: A Case Study on the Paternò–Büchi Reaction, *Z. Phys. Chem.*, 2013, **227**, 1421–1433.

24 S. Maeda, R. Saito and K. Morokuma, Finding minimum structures on the seam of crossing in reactions of type A + B → X: Exploration of nonadiabatic ignition pathways of unsaturated hydrocarbons, *J. Phys. Chem. Lett.*, 2011, **2**, 852–857.

25 S. Maeda, Y. Harabuchi, T. Taketsugu and K. Morokuma, Systematic Exploration of Minimum Energy Conical Intersection Structures near the Franck–Condon Region, *J. Phys. Chem. A*, 2014, **118**, 12050–12058.

26 P. M. Zimmerman, Growing string method with interpolation and optimization in internal coordinates: Method and examples, *J. Chem. Phys.*, 2013, **138**, 1–11.

27 P. Zimmerman, Reliable transition state searches integrated with the growing string method, *J. Chem. Theory Comput.*, 2013, **9**, 3043–3050.
28 P. M. Zimmerman, Single-ended transition state finding with the growing string method, *J. Comput. Chem.*, 2015, **36**, 601–611.
29 A. L. Dewyer and P. M. Zimmerman, Finding reaction mechanisms, intuitive or otherwise, *Org. Biomol. Chem.*, 2017, 501–504.
30 P. M. Zimmerman, Automated discovery of chemically reasonable elementary reaction steps, *J. Comput. Chem.*, 2013, **34**, 1385–1392.
31 P. M. Zimmerman, Navigating molecular space for reaction mechanisms: an efficient, automated procedure, *Mol. Simul.*, 2015, **41**, 43–54.
32 F. I. S. R. Srinivasan and R. Eisenberglk, Energy Level of the First Excited Singlet State of 1,3-Butadiene, *J Am Chem Soc*, 1965, **1735**, 1964–1965.
33 M. J. Bearpark, M. Deumal, M. A. Robb, T. Vreven, N. Yamamoto, M. Olivucci, F. Bernardi, C. G. Ciamician and V. Selmi, Modeling Photochemical [4 + 4] Cycloadditions : Conical Intersections Located with CASSCF for Butadiene + Butadiene, 1997, **7863**, 709–718.
34 D. R. Yarkony, Nonadiabatic Quantum Chemistry — Past , Present , and Future, *Chem. Rev.*, 2012, **112**, 481–498.
35 M. J. Bearpark, M. a. Robb and H. Bernhard Schlegel, A direct method for the location of the lowest energy point on a potential surface crossing, *Chem. Phys. Lett.*, 1994, **223**, 269–274.
36 F. Sicilia, L. Blancafort, M. J. Bearpark and M. a Robb, New Algorithms for Optimizing and Linking Conical Intersection Points, *J. Chem. Theory Comput.*, 2008, **4**, 257–266.
37 T. W. Keal, A. Koslowski and W. Thiel, Comparison of algorithms for conical intersection optimisation using semiempirical methods, *Theor. Chem. Acc.*, 2007, **118**, 837–844.
38 S. Ruiz-Barragan, M. A. Robb and L. Blancafort, Conical intersection optimization based on a double Newton-Raphson algorithm using composed steps, *J. Chem. Theory Comput.*, 2013, **9**, 1433–1442.
39 T. Chachiyo and J. H. Rodriguez, A direct method for locating minimum-energy crossing points (MECPs) in spin-forbidden transitions and nonadiabatic reactions, *J. Chem. Phys.*, 2005, **123**, 0–9.
40 L. De Vico, M. Olivucci and R. Lindh, New general tools for constrained geometry optimizations, *J. Chem. Theory Comput.*, 2005, **1**, 1029–1037.
41 F. Sicilia, L. Blancafort, M. J. Bearpark and M. A. Robb, Quadratic description of conical intersections: Characterization of critical points on the extended seam, *J. Phys. Chem. A*, 2007, **111**, 2182–2192.
42 A. Cembran, F. Bernardi, M. Olivucci and M. Garavelli, Counterion Controlled Photoisomerization of Retinal Chromophore Models: a Computational Investigation., *J. Am. Chem. Soc.*, 2004, **126**, 16018–16037.
43 B. G. Levine, J. D. Coe and T. J. Martínez, Optimizing Conical Intersections without Derivative Coupling Vectors: Application to Multistate Multireference Second-Order Perturbation Theory (MS-CASPT2), *J. Phys. Chem. B*, 2008, **112**, 405–413.
44 D. Passerone and T. Laino, Exploring conical intersection spaces using pseudo-dynamics and band optimization : a novel strategy, 2005, **169**, 305–308.
45 T. Laino and D. Passerone, Pseudo-dynamics and band optimizations : shedding light into conical intersection seams, 2004, **389**, 1–6.

46 T. Mori and T. J. Martínez, Exploring the conical intersection seam: The seam space nudged elastic band method, *J. Chem. Theory Comput.*, 2013, **9**, 1155–1163.
47 M. Jafari and P. M. Zimmerman, Reliable and efficient reaction path and transition state finding for surface reactions with the growing string method, *J. Comput. Chem.*, 2017, 645–658.
48 B. Peters, A. Heyden, A. T. Bell and A. Chakraborty, A growing string method for determining transition states: Comparison to the nudged elastic band and string methods, *J. Chem. Phys.*, 2004, **120**, 7877–7886.
49 M. Garavelli, P. Celani, M. Fato, M. J. Bearpark, B. R. Smith, M. Olivucci and M. a. Robb, Relaxation Paths from a Conical Intersection: The Mechanism of Product Formation in the Cyclohexadiene/Hexatriene Photochemical Interconversion, *J. Phys. Chem. A*, 1997, **101**, 2023–2032.
50 P. Celani, M. a. Robb, M. Garavelli, F. Bernardi and M. Olivucci, Geometry optimisation on a hypersphere. Application to finding reaction paths from a conical intersection, *Chem. Phys. Lett.*, 1995, **243**, 1–8.
51 M. Garavelli, F. Bernardi, A. Cembran, O. Castaño, L. M. Frutos, M. Merchán and M. Olivucci, Cyclooctatetraene Computational Photo- and Thermal Chemistry: A Reactivity Model for Conjugated Hydrocarbons, *J. Am. Chem. Soc.*, 2002, **124**, 13770–13789.
52 I. Fdez. Galván, M. G. Delcey, T. B. Pedersen, F. Aquilante and R. Lindh, Analytical State-Average Complete-Active-Space Self-Consistent Field Nonadiabatic Coupling Vectors: Implementation with Density-Fitted Two-Electron Integrals and Application to Conical Intersections, *J. Chem. Theory Comput.*, 2016, **12**, 3636–3653.
53 M. Garavelli, F. Bernardi, A. Cembran, O. Castaño, L. M. Frutos, M. Merchán and M. Olivucci, Cyclooctatetraene Computational Photo- and Thermal Chemistry: A Reactivity Model for Conjugated Hydrocarbons, *J. Am. Chem. Soc.*, 2002, **124**, 13770–13789.
54 B. Mignolet, B. F. E. Curchod and T. J. Martínez, Rich Athermal Ground-State Chemistry Triggered by Dynamics through a Conical Intersection, *Angew. Chemie Int. Ed.*, 2016, **55**, 14993–14996.
55 S. Althorpe, S. C. Althorpe and G. A. Worth, *Quantum Dynamics at Conical Intersections*, 2004.
56 J. Quenneville, M. Ben-Nun and T. J. Martínez, Photochemistry from first principles - advances and future prospects, *J. Photochem. Photobiol. a-Chemistry*, 2001, **144**, 229–235.
57 G. Tomasello, F. Ogliaro, M. J. Bearpark, M. A. Robb and M. Garavelli, Modeling the Photophysics and Photochromic Potential of 1,2-Dihydronaphthalene (DHN): A Combined CASPT2//CASSCF-Topological and MMVB-Dynamical Investigation, *J. Phys. Chem. A*, 2008, **112**, 10096–10107.
58 J. P. Malhado and J. T. Hynes, Non-adiabatic transition probability dependence on conical intersection topography, *J. Chem. Phys.*, , DOI:10.1063/1.4967259.
59 A. S. Michael S. Schuurman, Dynamics at Conical Intersections, *Annu. Rev. Phys. Chem.*, 2018, **69**, 427–450.
60 J. Quenneville, T. J. Martı, M. Ben-Nun, J. Quenneville, T. J. Martínez and T. J. Martı, Ab Initio Multiple Spawning: Photochemistry from First Principles Quantum Molecular Dynamics, *J. Phys. Chem. A*, 2000, **104**, 5161–5175.
61 H. Guo and D. R. Yarkony, Accurate nonadiabatic dynamics, *Phys. Chem. Chem. Phys.*, 2016, **18**, 26335–26352.

62 S. Maeda, K. Ohno and K. Morokuma, Updated branching plane for finding conical intersections without coupling derivative vectors, *J. Chem. Theory Comput.*, 2010, **6**, 1538–1545.
63 J. A. Kammeraad and P. M. Zimmerman, Estimating the Derivative Coupling Vector Using Gradients, *J. Phys. Chem. Lett.*, 2016, 5074–5079.
64 G. a Worth and L. S. Cederbaum, Beyond Born-Oppenheimer: molecular dynamics through a conical intersection., *Annu. Rev. Phys. Chem.*, 2004, **55**, 127–158.
65 J. Baker, A. Kessi and B. Delley, The generation and use of delocalized internal coordinates in geometry optimization, *J. Chem. Phys.*, 1996, **105**, 192–212.
66 J. Baker, Constrained optimization in delocalized internal coordinates, *J. Comput. Chem.*, 1997, **18**, 1079–1095.
67 P. Zimmerman, molecularGSM, https://github.com/ZimmermanGroup/molecularGSM.
68 C. G. Broyden, The Convergence of a Class of Double-rank Minimization Algorithms 1. General Considerations, *IMA J. Appl. Math.*, 1970, **6**, 76–90.
69 R. Fletcher, A new approach to variable metric algorithms, *Comput. J.*, 1970, **13**, 317–322.
70 D. Goldfarb, A family of variable-metric methods derived by variational means, *Math. Comput.*, 1970, **24**, 23–23.
71 D. F. Shanno, Conditioning of quasi-Newton methods for function minimization, *Math. Comput.*, 1970, **24**, 647–647.
72 H.-J. J. Werner, P. J. Knowles, G. Knizia, F. R. Manby, M. Schutz and M. Schutz, Molpro: A general-purpose quantum chemistry program package, *Wiley Interdiscip. Rev. Comput. Mol. Sci.*, 2012, **2**, 242–253.
73 S. Wilsey and K. N. Houk, H-vinyl conical intersections for dienes: A mechanism for the photochemical hula twist, *Photochem. Photobiol.*, 2002, **76**, 616–621.
74 M. Ben-Nun and T. J. Martínez, Photodynamics of ethylene: ab initio studies of conical intersections, *Chem. Phys.*, 2000, **259**, 237–248.
75 M. J. T. Jordan and S. H. Kable, Roaming Reaction Pathways Along Excited States, *Science (80-.).*, 2012, **335**, 1054–1055.
76 R. S. H. Liu, Photoisomerization by hula-twist: A fundamental supramolecular photochemical reaction, *Acc. Chem. Res.*, 2001, **34**, 555–562.
77 W. Fuß, C. Kosmidis, W. E. Schmid and S. A. Trushin, The photochemical cis-trans isomerization of free stilbene molecules follows a hula-twist pathway, *Angew. Chemie - Int. Ed.*, 2004, **43**, 4178–4182.
78 J. Quenneville and T. J. Martı, Ab Initio Study of Cis - Trans Photoisomerization in Stilbene and Ethylene, *J. Phys. Chem. A*, 2003, **107**, 829–837.
79 I. N. Ioffe and A. A. Granovsky, Photoisomerization of stilbene: The detailed XMCQDPT2 treatment, *J. Chem. Theory Comput.*, 2013, **9**, 4973–4990.
80 J. E. Norton and K. N. Houk, H/vinyl conical intersections of hexatrienes related to the hula-twist photoisomerization, *Mol. Phys.*, 2006, **104**, 993–1008.
81 I. M. Pendleton, M. H. Pérez-temprano, M. S. Sanford and P. M. Zimmerman, Experimental and Computational Assessment of Reactivity and Mechanism in C(sp^3)-N Bond-Forming Reductive Elimina- tion from Palladium (IV), *J. Am. Chem. Soc.*, 2016, **138**, 1–12.
82 A. J. Nett, W. Zhao, P. M. Zimmerman and J. Montgomery, Highly Active Nickel Catalysts for C–H Functionalization Identified through Analysis of Off-Cycle Intermediates, *J. Am. Chem.*

Soc., 2015, **137**, 7636–7639.
83 A. J. Nett, J. Montgomery and P. M. Zimmerman, Entrances, Traps, and Rate-Controlling Factors for Nickel-Catalyzed C − H Functionalization, *ACS Catal.* 2017, **7**, 7352-7362.
84 A. L. Dewyer and P. M. Zimmerman, Simulated Mechanism for Palladium-Catalyzed, Directed γ - Arylation of Piperidine, *ACS Catal.* **2017**, *7*, 5466-5477.
85 Y. Y. Khomutnyk, A. J. Arguelles, G. A. Winschel, Z. Sun, P. M. Zimmerman and P. Nagorny, Studies of the Mechanism and Origins of Enantioselectivity for the Chiral Phosphoric Acid-Catalyzed Stereoselective Spiroketalization Reactions, *J. Am. Chem. Soc.*, 2016, **138**, 444–456.
86 J. H. Tay, A. J. Argüelles, M. D. Demars, P. M. Zimmerman, D. H. Sherman and P. Nagorny, Regiodivergent Glycosylations of 6-Deoxy-erythronolide B and Oleandomycin-Derived Macrolactones Enabled by Chiral Acid Catalysis, *J. Am. Chem. Soc.*, 2017, **139**, 8570–8578.
87 M. L. Smith, A. K. Leone, P. M. Zimmerman and A. J. McNeil, Impact of Preferential π-Binding in Catalyst-Transfer Polycondensation of Thiazole Derivatives, *ACS Macro Lett.*, 2016, 1411–1415.

Table of contents

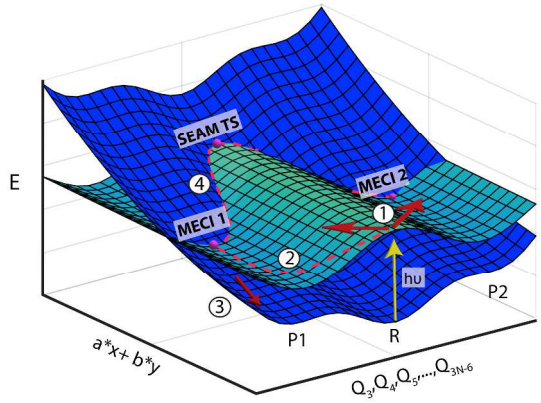

A new reaction discovery technique for photochemical reactions is herein used to explore complex intersections and predict product selectivity.